Chapter Nine

Quantum Monte Carlo Applied To the Spin-1 Easy-Plane Ferromagnet $CsNiF_3$

9.1 Introduction

In Chapter 8, the inadequacy of classical statistical mechanics using sG phenomenology for the description of spin-$\frac{1}{2}$ CHAB was demonstrated. For the sG theory to fit approximately to the experimental data, a renormalization of the sG rest mass was necessary. This renormalization has been attributed to quantum effects added to the sG theory, using the theory given by Maki (1981) and Maki and Takayama 1979. The quantum Monte Carlo method was used to quantize the full Hamiltonian from the start, rather than quantizing the classical sG limit of the full classical Hamiltonian. Moderate agreement with experimental data was obtained.

In this chapter, a similar calculation is presented for the spin-1 easy-plane ferromagnet $CsNiF_3$. Although the general formalism used here will be as described in Chapter 7, there are some differences from the spin-$\frac{1}{2}$ case. For instance, isotropic exchange plus a single ion anistropy will be used instead of anisotropic exchange. But the major difference will be that a spin-1 model in the checkerboard decomposition in principle can have $(2S + 1)^4 = 81$ possible vertices (all of these may not be allowed). At each site in the 2-D lattice there will be a classical spin variable which can have the three values -1, 0 or +1. The spin flipping algorithm will be modified from the spin-$\frac{1}{2}$ case to allow for the greater number of configurational possibilities. The rest of the calculation, for instance, the calculation of thermodynamic expectation values, is the same as for the spin-$\frac{1}{2}$ case as described in Chapter 7.

9.2 Vertex Energies for a Spin-1 Model with Exchange Anisotropy

In the notation of Chapter 7, the following two-body spin-1 Hamiltonian is considered first,

$$\hat{H}^{o}_{n,n+1} = -J_z \hat{S}^z_n \hat{S}^z_{n+1} - \frac{1}{2} g\mu_B B_B (\hat{S}^z_n + \hat{S}^z_{n+1}) \tag{9-1a}$$

$$\hat{V}_{n,n+1} = -J_x \hat{S}^x_n \hat{S}^x_{n+1} - J_y \hat{S}^y_n \hat{S}^y_n \quad . \tag{9-1b}$$

$\hat{S}^x_n$, $\hat{S}^y_n$, $\hat{S}^z_n$ are spin-1 operators, satisfying the fundamental commutation relation

$$[\hat{S}^i_n, \hat{S}^j_n] = i\, \delta_{nm} \hat{S}^k_n \quad , \quad i, j, k \text{ cyclic} \quad , \tag{9-2}$$

and otherwise described by spin-1 algebra. J_x, J_y and J_z are arbitrary exchange constants and B_z is the applied field. This Hamiltonian is presented as a practice example. Later we will include a single ion anisotropy.

The matrix elements as in equation (7-12) are to be calculated, and we will use eigenstates of $\hat{S}^z_n$ operators. This makes the matrix elements of $\hat{H}^{o}_{n,n+1}$ trivial, such that the vertex weight $w_{n,r}$ is

$$w_{n,r} = e^{-\beta E_{n,r}} = e^{-\beta E^{o}_{n,r}} \langle S_{n,r} S_{n+1,r} | e^{-\beta \hat{V}_{n,n+1}} | S_{n,r+1} S_{n+1,r+1} \rangle \tag{9-3a}$$

where

$$E^{o}_{n,r} = -\frac{1}{2m}[J_z (S_{n,r} S_{n+1,r} + S_{n,r+1} S_{n+1,r+1}) + \frac{1}{2} g\mu_B B_z (S_{n,r} + S_{n+1,r} + S_{n,r+1} + S_{n+1,r+1})] \tag{9-3b}$$

This is the same $E^{o}_{n,r}$ as for the spin-$\frac{1}{2}$ case. To find the remaining matrix element, we will consider expanding and re-summing the exponential series for $\hat{M} \equiv \frac{-\beta}{m} \hat{V}_{n,n+1}$. For simplicity of notation, consider n = 1, and write x_n and y_n in place of $\hat{S}^{x}_{n}$ and $\hat{S}^{y}_{n}$. Making the definition of dimensionless parameters

$$K_{x,y,z} \equiv \frac{\beta}{m} J_{x,y,z} \quad , \tag{9-4}$$

we have

$$e^{\hat{M}} = \sum_{p=0}^{\infty} \frac{1}{p!} \hat{M}^{p} \quad , \quad \text{where } \hat{M} = K_x x_1 x_2 + K_y y_1 y_2 \quad . \tag{9-5}$$

It is possible to express the powers of $\hat{M}$ in terms of simple combinations of the x_n and y_n operators. First, notice that $\hat{M}$ is symmetric in x and y; interchanging <u>all</u> x and y component indices does not change $\hat{M}$. Similarly, all powers of $\hat{M}$ will be symmetric in x and y. Therefore, we can use a notation

$$\hat{M} = K_x x_1 x_2 + \{x \leftrightarrow y\} \tag{9-6}$$

where $\{x \leftrightarrow y\}$ indicates a term as the first but with <u>all</u> x's and y's interchanged. Higher powers of $\hat{M}$ can be found by direct multiplication using spin-1 algebra, in particular, forming products from the 3 x 3 spin-1 matrices. As for the spin-$\frac{1}{2}$ case, it is easiest to consider the even power of $\hat{M}$ first. Starting with $\hat{M}^2$,

$$\hat{M}^2 = K_x^2 (xx)_1 (xx)_2 + K_x K_y (xy)_1 (xy)_2 + \{x \leftrightarrow y\} \quad . \tag{9-7}$$

Squaring equation (9-7) produces

$$\hat{M}^4 = (K_x^2)^2(xx)_1(xx)_2 + K_xK_y(K_x^2+K_y^2)(xy)_1(xy)_2 + K_x^2K_y^2(xxyy)_1(xxyy)_2$$

$$+ K_x^2K_y^2(xyyx)_1(xyyx)_2 + \{x \leftrightarrow y\} \quad . \tag{9-8}$$

We have used some easily verified spin-1 identities,

$$x_n^3 = x_n \quad , \quad y_n^3 = y_n$$

$$(xy)_n^2 = (yx)_n^2 = 0$$

$$(xyx)_n = (yxy)_n = 0 \quad , \tag{9-9}$$

It turns out that any even power of $\hat{M}$ can be written in terms of just the four operators seen in equation (9-8). We suppose that the pth power of $\hat{M}$ can be written (p even)

$$\hat{M}^p = a_p(xx)_1(xx)_2 + b_p(xy)_1(xy)_2 + c_p(xxyy)_1(xxyy)_2 + d_p(xyyx)_1(xyyx)_2$$

$$+ \{x \leftrightarrow y\} \quad . \tag{9-10}$$

Then multiplying by $\hat{M}^2$ leads to a similar expression for $\hat{M}^{p+2}$ (changing $p \to p + 2$ in 9-10), with the $(p + 2)$th coefficients related to the pth coefficients by

$$\begin{bmatrix} a \\ b \\ c \\ d \end{bmatrix}_{p+2} = \begin{bmatrix} K_x^2 & 0 & 0 & 0 \\ K_xK_y & K_y^2 & 0 & K_xK_y \\ K_y^2 & 0 & K_x^2+K_y^2 & 0 \\ 0 & K_xK_y & 0 & K_x^2 \end{bmatrix} \begin{bmatrix} a \\ b \\ c \\ d \end{bmatrix}_{p} \quad . \tag{9-11}$$

At this point, we need to iterate this transformation, starting from the initial condition for p = 2, from equation (9-7),

$$\vec{A}_{p=2} \equiv \begin{bmatrix} a \\ b \\ c \\ d \end{bmatrix}_2 = \begin{bmatrix} K_x^2 \\ K_x K_y \\ 0 \\ 0 \end{bmatrix} \quad . \qquad (9\text{-}12)$$

We will refer to the matrix in (9-11) as transformation T. Generally, then

$$\vec{A}_{p+2} = T \cdot \vec{A}_p \quad \text{or} \quad \vec{A}_p = T^{\frac{p-2}{2}} \cdot \vec{A}_2 \quad , \quad p \ \underline{\text{even}} \quad . \qquad (9\text{-}13)$$

Closed-form simple expressions for $\vec{A}_p$ can be found by making use of the eigenspectrum of T, and expanding $\vec{A}_2$ in terms of that eigenspectrum. Solving $T\vec{u} = \lambda\vec{u}$ leads to

$$\det(T - \lambda I) = \lambda(\lambda - K_x^2)(\lambda - K_x^2 - K_y^2)^2 = 0 \quad . \qquad (9\text{-}14)$$

One eigenvalue is degenerate. Unnormalized eigenvectors are

$$\vec{u}_1 = \begin{bmatrix} 0 \\ K_x^2 \\ 0 \\ -K_x K_y \end{bmatrix} \quad , \quad \lambda_1 = 0$$

$$\vec{u}_2 = \begin{bmatrix} 1 \\ 0 \\ -1 \\ -1 \end{bmatrix} \cdot K_x^2 \quad , \quad \lambda_2 = K_x^2$$

$$\vec{u}_3 = \begin{bmatrix} 0 \\ K_x K_y \\ 0 \\ K_x^2 \end{bmatrix} \quad , \quad \lambda_3 = K_x^2 + K_y^2$$

$$\vec{u}_4 = \begin{bmatrix} 0 \\ K_x K_y \\ K_x^2 \\ K_x^2 \end{bmatrix} \quad , \quad \lambda_4 = K_x^2 + K_y^2 \quad . \tag{9-15}$$

A quick calculation shows that the expansion of $\vec{A}_2$ is

$$\vec{A}_2 = \vec{u}_2 + \vec{u}_4 \quad . \tag{9-16}$$

Applying T to this leads easily to

$$\vec{A}_p = \lambda_2^{\frac{p-2}{2}} \cdot \vec{u}_2 + \lambda_4^{\frac{p-2}{2}} \cdot \vec{u}_4 \quad , \tag{9-17}$$

which when written out in components gives the expansion coefficients for $\hat{M}^p$, p even,

$$a_p = K_x^p$$

$$b_p = K_x K_y \left(K_x^2 + K_y^2\right)^{\frac{p-2}{2}}$$

$$c_p = d_p = K_x^2 \left(K_x^2 + K_y^2\right)^{\frac{p-2}{2}} - K_x^{p-2} \quad . \tag{9-18}$$

These are substituted back into equations (9-10) and (9-5), such that we make use of the exponential series sums

$$\sum_{p=2,4}^{\infty} \frac{1}{p!}\, a_p = \cosh K_x - 1$$

$$\sum_{p=2,4,}^{\infty} \frac{1}{p!}\, b_p = \frac{K_x K_y}{K_x^2+K_y^2} (\cosh K_{xy} - 1)$$

$$\sum_{p=2,4,}^{\infty} \frac{1}{p!}\, c_p = \frac{K_x^2}{K_x^2+K_y^2} (\cosh K_{xy} - 1) - (\cosh K_x - 1) \quad , \tag{9-19}$$

where

$$K_{xy} \equiv (K_x^2+K_y^2)^{1/2} \quad . \tag{9-20}$$

Therefore, the sum of the even powers of $\hat{M}$ in the expansion of $e^{\hat{M}}$ (equation 9-5) is

$$\sum_{p=0,2,4,}^{\infty} \frac{1}{p!}\, \hat{M}^p = 1 + (\cosh K_x - 1)(xx)_1(xx)_2 + \frac{K_x K_y}{K_{xy}^2} (\cosh K_{xy} - 1)(xy)_1(xy)_2$$

$$+ \frac{K_x^2}{K_{xy}^2} (\cosh K_{xy} - 1) - (\cosh K_x - 1)](xxyy)_1(xxyy)_2 + (xyyx)_1(xyyx)_2$$

$$+ \{x \leftrightarrow y\} \quad . \tag{9-21}$$

The odd powers of $\hat{M}$ are obtained easily from the even powers by $\hat{M}^{p+1} = \hat{M}^p \cdot \hat{M}$, where p = even. After some further straightforward algebra, one finds

$$\sum_{p=1,3,5,}^{\infty} \frac{1}{p!} \hat{M}^p = [\frac{K_x}{K_{xy}} \sinh K_{xy} - \sinh K_x][(xxy)_1(xxy)_2 + (yxx)_1(yxx)_2]$$

$$+ \sinh K_x \cdot (x_1 x_2) + \{x \leftrightarrow y\} \quad . \tag{9-22}$$

The sum of these last two equations is $e^{\hat{M}}$. From these expressions the matrix elements which determine vertex energies can be obtained. They are given in Appendix C. It is noted here that the even powers of $\hat{M}$ determine 25 nonzero vertex weights, while the odd powers determine 16 nonzero vertex weights, for a total of 41 allowed vertices, provided $J_x \neq J_y$. If $J_x = J_y$, then the even powers give 11 allowed vertices, while the odd powers give 8 allowed vertices, for a total of 19. The number of allowed vertices in the isotropic case is greatly reduced from the possible 81.

For an arbitrary-S <u>isotropic</u> model ($J_x = J_y$), the only allowed vertices are those which conserve total magnetization, since $\hat{V}_{n,n+1}$ would then be $-J_x(\hat{S}_n^+\hat{S}_{n+1}^- + \hat{S}_n^-\hat{S}_{n+1}^+)$. For the matrix element $\langle S_1 S_2 | e^{\hat{M}} | S_1 S_2 \rangle$, counting the number of ways one can satisfy $S_1+S_2 = S_1'+S_2'$, leads to the number of allowed vertices being

$$N_v = 2(1 + 2^2 + 3^2 + \ldots + (2S)^2) + (2S+1)^2 \quad . \tag{9-23}$$

So, for example, a spin-$\frac{3}{2}$ isotropic model will have 44 allowed vertices out of 256 possible.

9.3 <u>Vertex Energies of a Spin-1 Model with Single Ion Anisotropy</u>

The above was an example calculation. We would like to add a single site anisotropy term to $\hat{V}_{n,n+1}$ of the form $\frac{1}{2}A(\hat{S}_n^y\hat{S}_n^y + \hat{S}_{n+1}^{y2}\hat{S}_{n+1}^y)$, since this is the type of easy-plane interaction believed to be applicable for $CsNiF_3$.

Unfortunately, adding this term and repeating the above calculation leads to considerable complications in the algebra, especially because now $\hat{M}$ will not be symmetric with respect to x and y indices. In addition, the operator T is described by a 12 x 12 matrix. A different way of splitting $\hat{H}_{n,n+1}$ into two parts leads to simpler algebra. One thing to try is to place all the (isotropic) exchange interaction into $\hat{V}_{n,n+1}$ and then $\hat{H}^{o}_{n,n+1}$ will involve the magnetic field and anisotropy field,

$$\hat{H}^{o}_{n,n+1} = \frac{1}{2}A(\hat{S}^{y}_{n}\hat{S}^{y}_{n} + \hat{S}^{y}_{n+1}\hat{S}^{y}_{n+1}) - \frac{1}{2}g\mu_{B}B_{z}(\hat{S}^{z}_{n} + \hat{S}^{z}_{n+1}) \tag{9-24a}$$

$$\hat{V}_{n,n+1} = -J\vec{\hat{S}}_{n}\cdot\vec{\hat{S}}_{n+1} \tag{9-24b}$$

For this breakup of $\hat{H}_{n,n+1}$, the algebra introduced in Section 9.2 works very easily for $\hat{H}^{o}_{n,n+1}$, except that we cannot use the $x \leftrightarrow y$ symmetry. However, $\hat{H}^{o}_{n,n+1}$ is a sum of commuting operators, so that we have

$$\exp(\frac{-\beta}{2m}\hat{H}^{o}_{n,n+1}) = \exp(-\alpha y^{2}_{n} + b_{z}z_{n})\exp(-\alpha y^{2}_{n+1} + b_{z}z_{n+1}) \tag{9-25}$$

where, in this chapter, α and b_{z} are

$$\alpha \equiv \frac{\beta A}{4m} \quad , \quad b_{z} \equiv \frac{\beta}{4m}g\mu_{B}B_{z} \quad . \tag{9-26}$$

Putting $\hat{M} = -\alpha y^{2}_{n} + b_{z}z_{n}$, we just note that the calculations are simplified here and for $\hat{V}_{n,n+1}$ by finding higher powers of $\hat{M}$ symmetrically using an anticommuntator,

$$\hat{M}^{p+1} = \frac{1}{2}\{\hat{M}, \hat{M}^{p}\} \quad . \tag{9-27}$$

Also, in these cases it is not necessary to consider even powers of $\hat{M}$ separately from odd powers; it is most efficent to work with the transformation T that takes the operator coefficients for $\hat{M}^{p}$ to the coefficents

for $\hat{M}^{p+1}$. With these modifications, the spin-1 algebra leads to the result

$$\exp(-\alpha y_n^2 + b_z z_n) = 1 + (e^{-\alpha} - 1)(y_n^2) + b_z \gamma^{-1} e^{-\frac{1}{2}\alpha} \sinh \gamma(z_n)$$

$$+ [e^{-\frac{1}{2}\alpha}(\cosh \gamma + \frac{1}{2}\alpha\gamma^{-1} \sinh \gamma) - 1[(xyyx)_n$$

$$+ [e^{-\frac{1}{2}\alpha}(\cosh \gamma - \frac{1}{2}\alpha\gamma^{-1} \sinh \gamma) - e^{-\alpha}](yxxy)_n \quad , \qquad (9\text{-}28a)$$

where

$$\gamma \equiv (b_z^2 + \frac{1}{4}\alpha^2)^{\frac{1}{2}} \quad . \qquad (9\text{-}28b)$$

The corresponding calculation for $\hat{V}_{n,n+1}$ is more complicated, but similar. An operator expression for $\exp(\frac{-\beta}{m}\hat{V}_{n,n+1})$ is given in Appendix C, along with the 19 nonzero matrix elements. For arbitrary S, this isotropic interaction has N_v nonzero matrix elements, as given in equation (9-23). Upon multiplying the matrices for $\exp(-\frac{\beta}{2m}\hat{H}^{\circ}_{n,n+1})$ and $\exp(-\frac{\beta}{m}\hat{V}_{n,n+1})$ to obtain the net vertex weight in equation (7-12), it is found that there are 41 nonzero vertices for spin-1. Whereas the spin-$\frac{1}{2}$ vertices which were allowed in the 8 vertex model had an even number of $+\frac{1}{2}$'s, in this spin-1 41 vertex model the allowed vertices have an even number of zeros (a vertex can be combinations of -1, 0 and +1 spins). For reasons analogous to those for spin-$\frac{1}{2}$ models, Monte Carlo flipping algorithms can be most efficiently designed for either 41 or 81 vertex models. In the 41 vertex model a combination of row, column and square "moves" can be used which always produce allowed states, while for the 81 vertex model one could use individual spin moves. Any number other than these are likely to be both inconvenient and inefficient, due to the generation of prohibited states.

This model Hamiltonian (equation 9-24) has 41 nonzero vertex weights provided $A \neq 0$, even if $B_z = 0$. As for CHAB, this is important since we want to study the thermodynamics as a function of the field B_z, with A held fixed. For $CsNiF_3$, the parameters believed to be appropriate are A = 9.0 K and J = 23.6 K (Steiner 1981, Steiner et al. 1983), for a quantum description. This is 38% anistropy, considerably larger than for CHAB, and it is expected that this should be a good 41 vertex model to work with, rather than a slightly perturbed 19 vertex model. This is the model we use to study $CsNiF_3$.

9.4 A Flipping Algorithm for the 41 Vertex Model

The 2-D classical system on which the Metropolis et al. algorithm is performed is an N x 2m lattice. At each site is a classical spin variable $S_{n,r}$ that has the three possible states -1, 0, +1. As for spin-$\frac{1}{2}$ there are periodic boundary conditions in both directions. Starting from any given allowed state of the entire system, we require a simple algorithm that has equal a priori probability of transition to any other allowed state. This new state is then accepted with probability 1 if $\Delta E < 0$ and probability $e^{-\beta\Delta E}$ if $\Delta E > 0$, where ΔE is the change in the effective energy of the 2-D lattice.

It is not obvious how to create such an algorithm. Instead, we can follow the example of the spin-$\frac{1}{2}$ problem and generate columns, rows and squares (in the "holes" in the checkerboard) along which spins are altered. In the spin-$\frac{1}{2}$ case, the allowed vertices in the 8 vertex model have an even number of $+\frac{1}{2}$'s. This necessitated changing the signs on spins in a vertex in pairs. This requirement resulted in there being only two final states possible for flipping a given column, row, or square (i.e. no change, or flip all spins). In the spin-1 case it is not so

simple. Starting from a given "path" (a column, row or square) of -1, 0 and +1 spins, a method is needed which ensures that all the allowed possible output states have equal a priori probabilities. A method is described below. Once a column, row or square is chosen, all output states for that set of spins will be made to be equally probable. But there is still a question of how to decide whether (and where) to do a column, row or square move, or some other move, such that all states of the entire system will have equal a priori transition probabilities (before testing ΔE to see whether the move should be accepted). Presently this question has not been answered.

A move is considered that will alter p spins along some path in the lattice. For a column move $p = 2m$, for a row move $p = N$, and for a square move $p = 4$. Any nearest neighbor pair of spins in the path belongs to a vertex; see Figure 9.1. If the number of zeroes in the pair is odd (even) before the attempted move, it must remain odd (even) after the move, since the allowed vertices in this 41 vertex model always have an even number of zeroes. This restriction limits the moves to two types:

1. "Unflipped": All zeroes in the path remain zero.
   All ±1's in the path go to +1 or -1 with equal probability.
2. "Flipped": All zeroes in the path go to +1 or -1 with equal probability.
   All ±1's in the path go to zero.

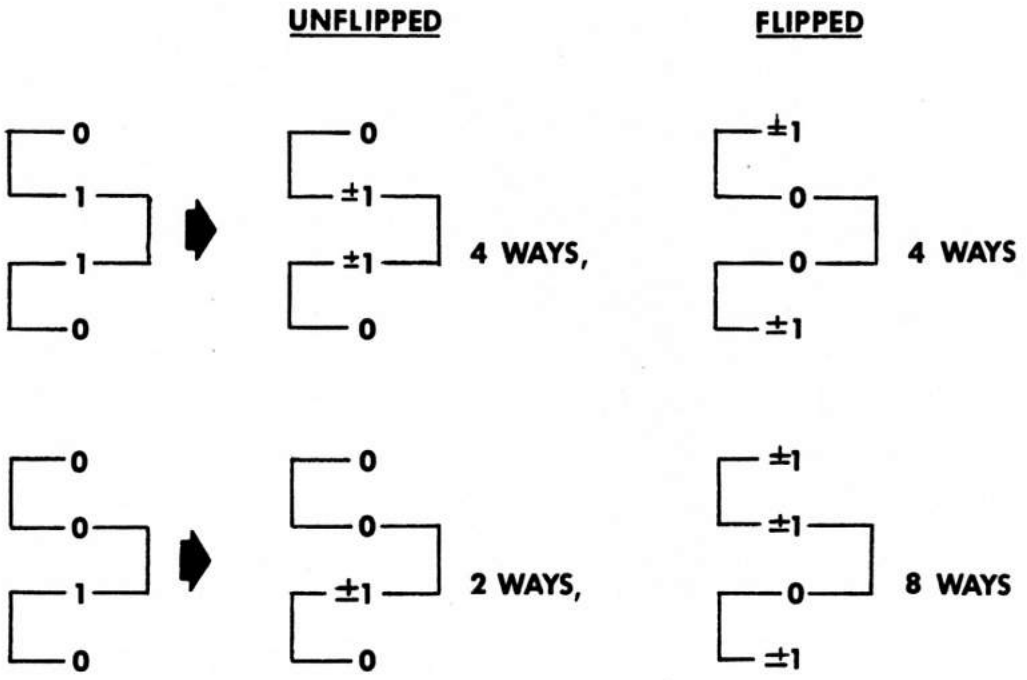

Figure 9.1 Typical unflipped and flipped moves, starting from a column with either an even or odd number of zeroes. In the top example, the unflipped and flipped transitions should be attempted with equal probability. In the bottom example, unflipped transitions should be attempted with probability 0.2 and flipped transitions should be attempted with probability 0.8, in order to make each of the 10 possible final states equally probably.

The decision whether to try the flipped or unflipped move is based on the number of zeroes N_0 along the path before the move. For a given initial path, there are 2^{N_0} flipped moves possible, and 2^{p-N_0} unflipped moves possible, for a total of $2^{N_0} + 2^{p-N_0}$ possible output states for the path. Therefore the flipped move should be attempted with probability $2^{N_0}/(2^{N_0} + 2^{p-N_0})$ and the unflipped move should be attempted with probability $2^{p-N_0}/(2^{N_0}+2^{p-N_0})$. In the absence of any interactions (all vertex weights equal), we have tested that this algorithm generates equal numbers of -1's, 0's and +1's in the lattice, using an approximately equal number of column, row and square paths at random locations.

9.4 Monte Carlo Details

This spin-1 simulation is less efficient than the spin-$\frac{1}{2}$ version, due to the larger number of vertices allowed, since one must make all allowed vertices possible within the algorithm. This has necessitated using a system of only 16 spins in order to reduce the computing time needed for the calculations. This was also necessary since much longer runs were needed, especially because of a strong tendency for the system to become stuck in some nonequilibrium trajectory. Possibly an annealing method would correct this problem, whereby the temperature would be lowered slowly to the desired temperature as the simulation progressed, rather than using an instantaneous "quenching" from high temperature.

For the $CsNiF_3$ parameters, in the temperature range $5 \leq T \leq 15$ and field range $0 \leq B_z \leq 10$ kG (B_z is the field in the easy plane), it is found that square flips have moderate acceptance rates ($\gtrsim 10\%$), while the acceptance rates for row and column flips are much smaller ($\ll 1\%$). This

is the case assuming that the simulation is done at a fixed value of mT; with this constraint the Trotter approximation errors at different temperatures should be of similar size. Naturally, then, one must use a larger lattice in the Trotter direction at lower temperatures. The data here was obtained using $mT \gtrsim 60$ Kelvin, and with only square flips, to improve the efficiency of the method. Of course it is not known whether this will severely inhibit the simulation from reaching all allowed states as it should, and it is not specifically known how to estimate the Trotter errors for a given value of mT (or J/mT).

The starting configuration of the 2-D lattice was taken to be the state with all $S_{n,r} = 0$. Vertex weights were calculated for a temperature 2T, and the Monte Carlo algorithm was applied for some 3000 to 5000 "steps", where a step involved attempting mN square flips at randomly chosen positions in the lattice. There are $\frac{1}{2}$ mN squares in the lattice to choose from, so this is effectively two sweeps through the lattice per step. This process created an initial configuration from which a Monte Carlo simulation was initiated, after recalculating the vertex weights for temperature T. The first 25% of these steps were discarded (64,000 steps), in order to allow the system to equilibrate. Then data was taken for 192,000 steps, after every step, from which the appropriate expectation values were computed, to obtain the internal energy, specific heat, magnetization and susceptibility, in manner identical to that done for the spin-$\frac{1}{2}$ problem. This data was divided into 6 groups of 32,000 steps for estimation of errors. Finally, the data obtained from five such runs was averaged to give the results shown here.

For zero applied field, the sequence of states generated tended to have a nonzero average magnetization, especially at low temperature,

because of the strong exchange between nearest neighbor spins. To circumvent this difficulty a global move was added to the algorithm, whereby all of the spins of the lattice are reversed in sign. At zero field this move is always accepted, and although there is no effect on the internal energy and specific heat, the average magnetization becomes zero, and the susceptibility is also corrected. At nonzero field the move is accepted with probability $e^{-\beta\Delta E}$ for $\Delta E > 0$, and probability 1 for $\Delta E \leq 0$, as for any other elementary move. This move was attempted once every step.

9.5 Results for $CsNiF_3$

In Figure 9.2 data vs. temperature is shown from the simulation for $CsNiF_3$, at three representative applied fields, B_z = 0, 5 and 10 kG. This represents only a fraction of the data since runs were performed at 1 K increments from 5 to 15 K, and for fields from 0 to 10 kG at 1 kG increments. Generally, however, the scatter in the data of Figure 9.2 is representative of the scatter at other applied fields. Unfortunately this scatter is considerable and makes interpretation of the data difficult. However, this length of run for the present algorithm was at the limit of reasonable cpu time (0.5 to 3 hours per data point).

In Figure 9.2b the differences $\Delta U = U(B_z) - U(0)$ and $\Delta C = C(B_z) - C(0)$ are shown, as was done for the spin-$\frac{1}{2}$ problem to attempt to isolate the specific heat contributions of excitations present only under application of the field. Again the scatter is appreciable and it is difficult to locate the position of the peak in $\Delta C(T)$ -- the amplitude of any peak is even more difficult to estimate. Data at the other fields is not much better. One more thing to do, however, is to plot ΔC vs. applied field, for fixed temperature, following Ramirez (1984). Again the soliton

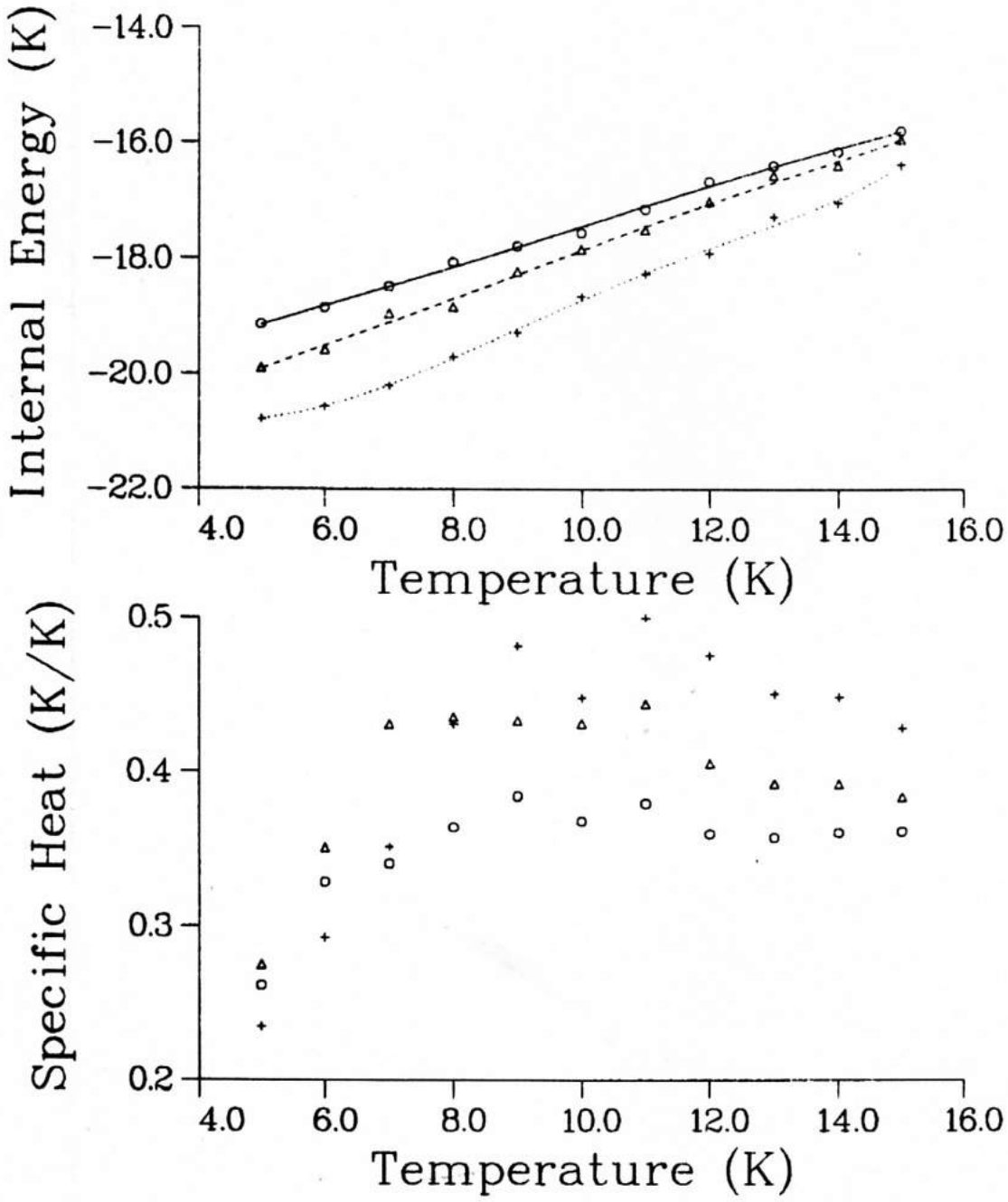

Figure 9.2a Internal energy and specific heat for $CsNiF_3$ parameters, vs. temperature. The data points are for fields 0.0 kG (0), 5.0 kG (Δ) and 10.0 kG (+). The curves are polynomial fits.

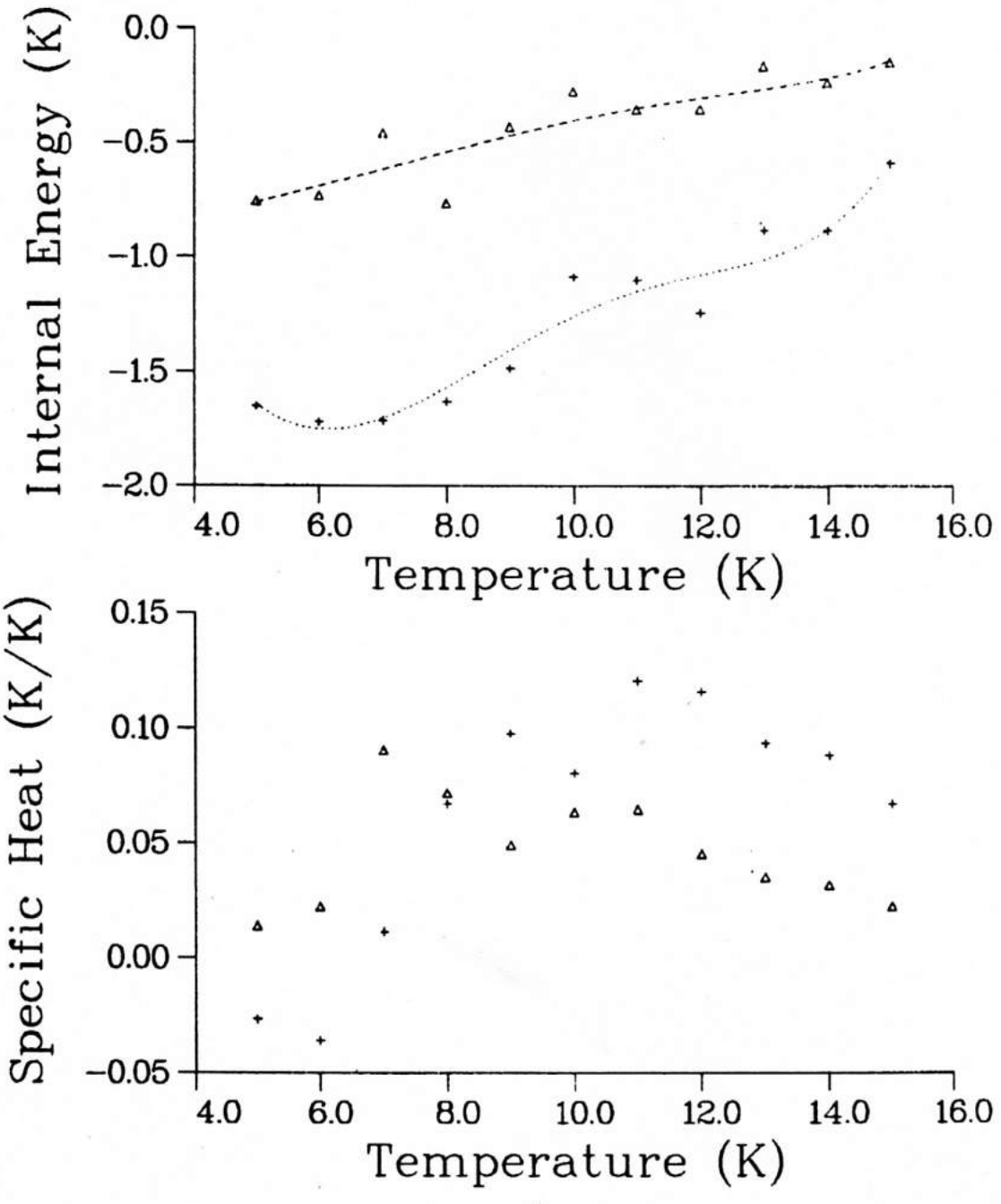

Figure 9.2b The differences ΔU and ΔC vs. temperature at fixed field, derived from 9.2a. The data points are for fields 5.0 kG (Δ) and 10.0 kG (+).

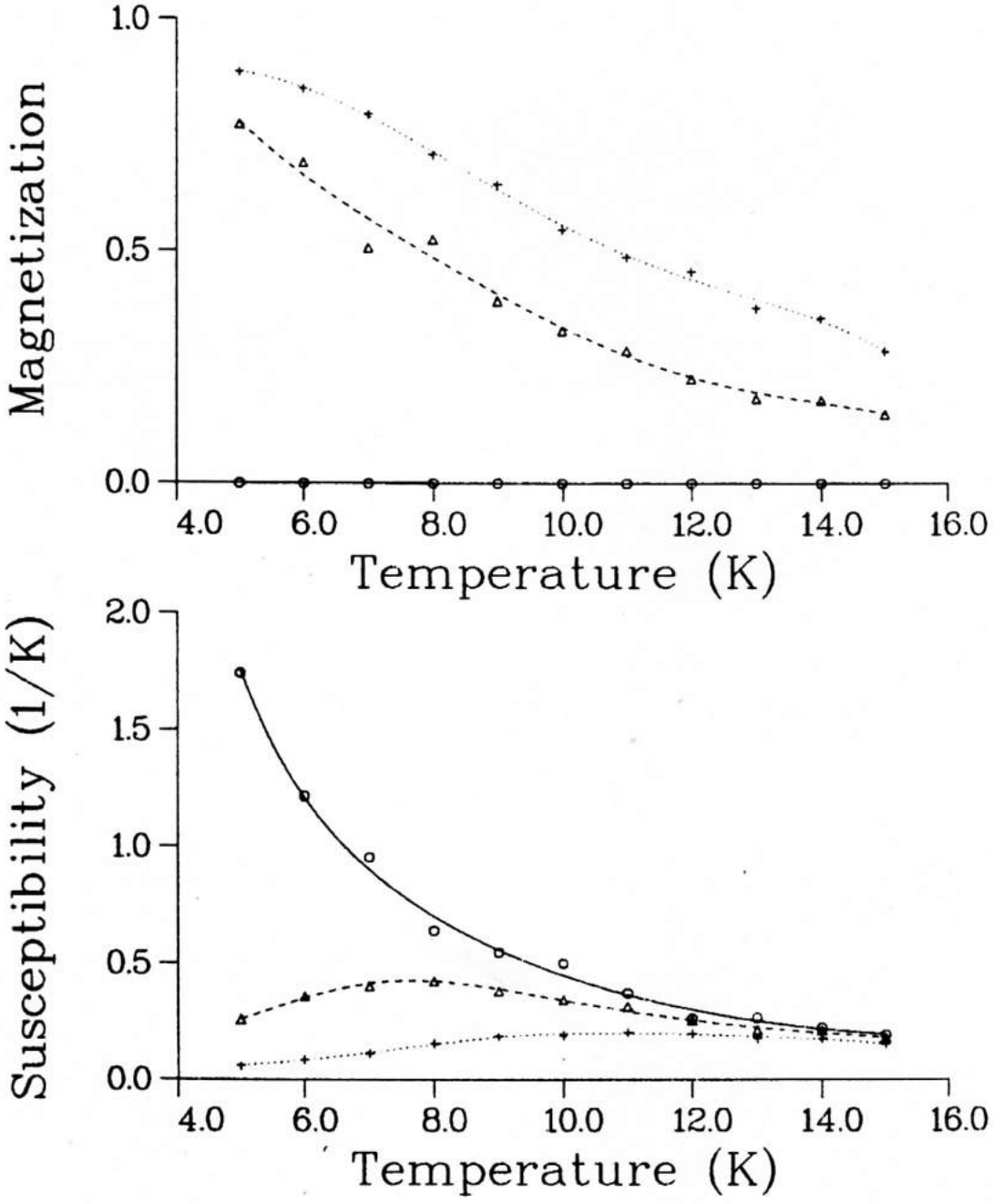

Figure 9.2c Magnetization and susceptibility for $CsNiF_3$ parameters, vs. temperature, for fields 0.0 kG (0), 5.0 kG (Δ) and 10.0 kG (+). The curves are polynomial fits.

picture predicts a peak in $\Delta C(B_z)$, whose position and height depend on temperature. Some representative low temperature data is shown in Figure 9.3. For the five curves shown (5,6,7,8 and 9 K), we can estimate that $\Delta C(B_z)$ peaks at fields 2,4,5,7 and 10 kG respectively, very roughly. In Figure 9.4 we show then the fields B_{peak} at which $\Delta C(B_z)$ peaks vs. the temperature squared, using these figures. A straight line fit to this data gives

$$B_{peak} \simeq 0.136\ T^2 - 1.35 \text{ (quantum M.C. data)} \quad , \tag{9-29}$$

where B is in kG and T is in Kelvin. The data from Ramirez and Wolf (1982) and Ramirez (1984) give

$$B_{peak} \simeq 0.131\ T^2 \text{ (Ramirez data)} \quad , \tag{9-30}$$

while the sG soliton picture predicts

$$B_{peak} = 0.62\ T^2 \quad . \tag{9-31}$$

The higher slope of the Ramirez data compared to sG theory has been attributed to a 31% reduction in the rest energy of the solitons, probably from quantum renormalization of the sG classical Hamiltonian. It is interesting that 9-29 and 9-30 have nearly the same slope; possibly this is coincidental, especially considering the quality of the M.C. data. Nevertheless, the M.C. algorithm does give B_{peak} approximately linearly proportional to T^2, consistent with experimental data and sG theory.

9.6 Comments on the Results

There is rough agreement between the M.C. data and the Ramirez experimental data for B_{peak} vs. T^2, but not so for the peak heights,

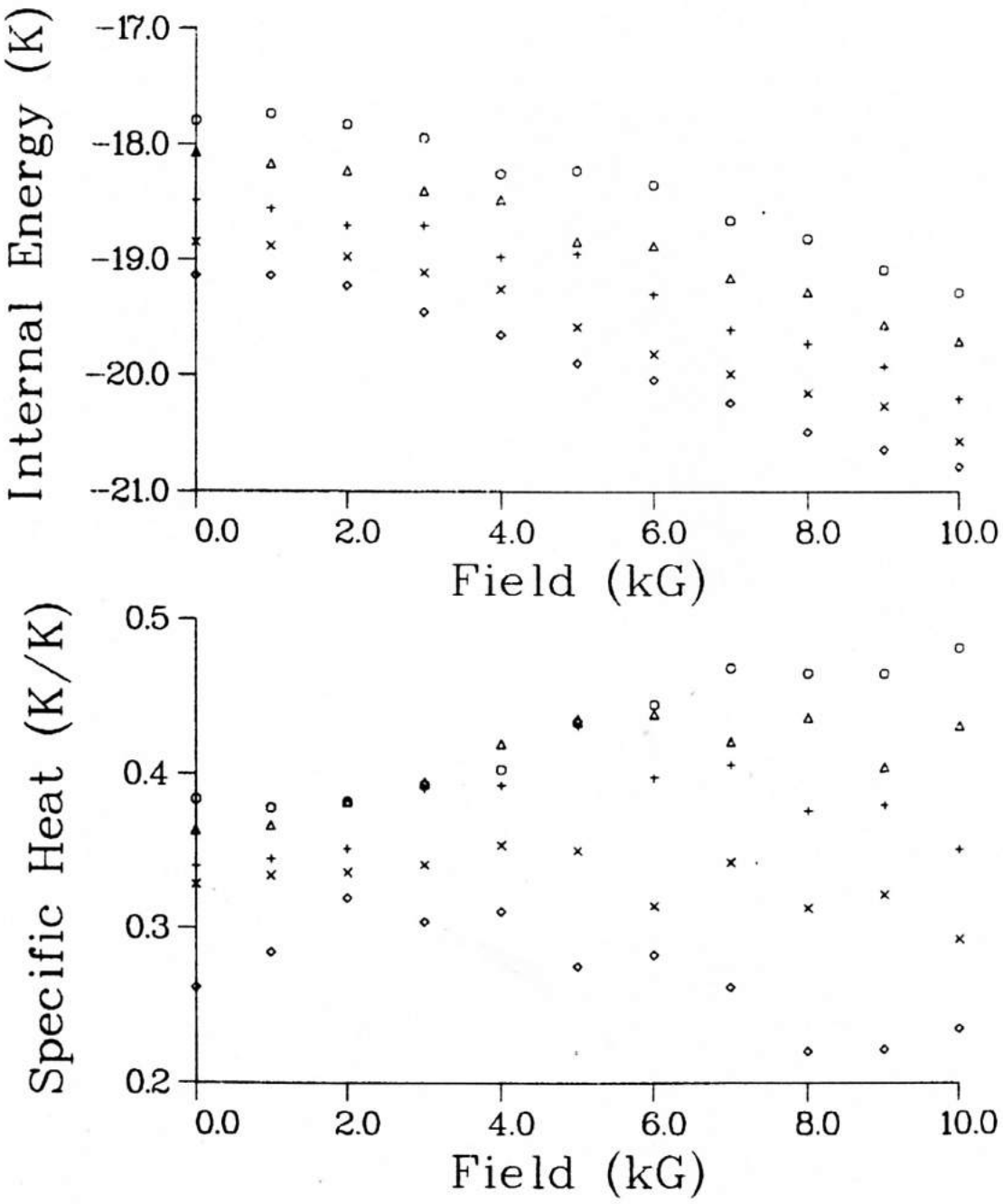

Figure 9.3a Internal energy and specific heat vs. applied field in the easy plane, for the $CsNiF_3$ parameters. The data points refer to temperature 9 K (0), 8 K (Δ), 7 K (+), 6 K (x) and 5 K (◊).

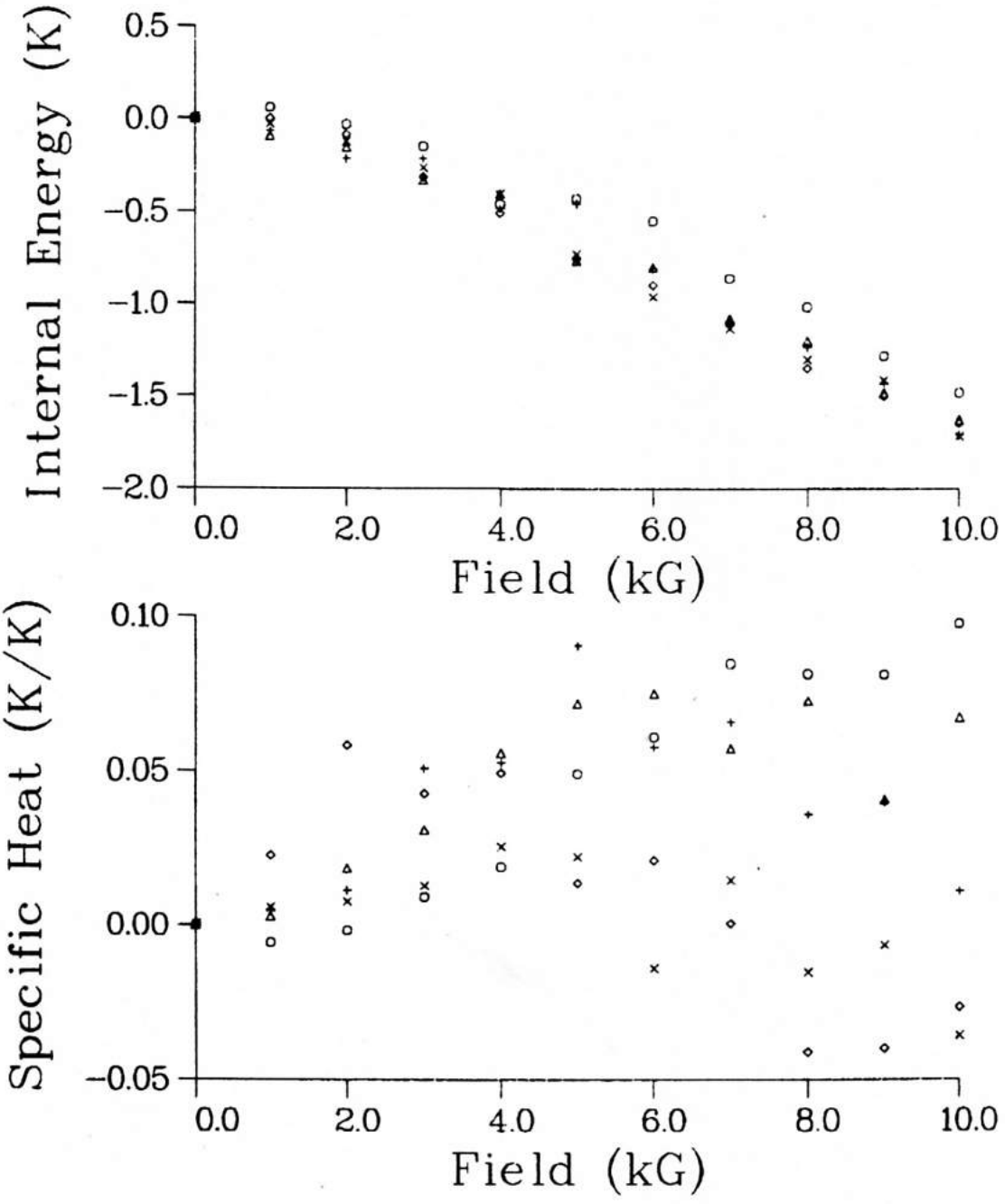

Figure 9.3b The differences ΔU and ΔC at fixed temperature, vs. field, derived from 9.3a. The data points refer to temperatures 9 K (0), 8 K (Δ), 7 K (+), 6 K (x) and 5 K (◇).

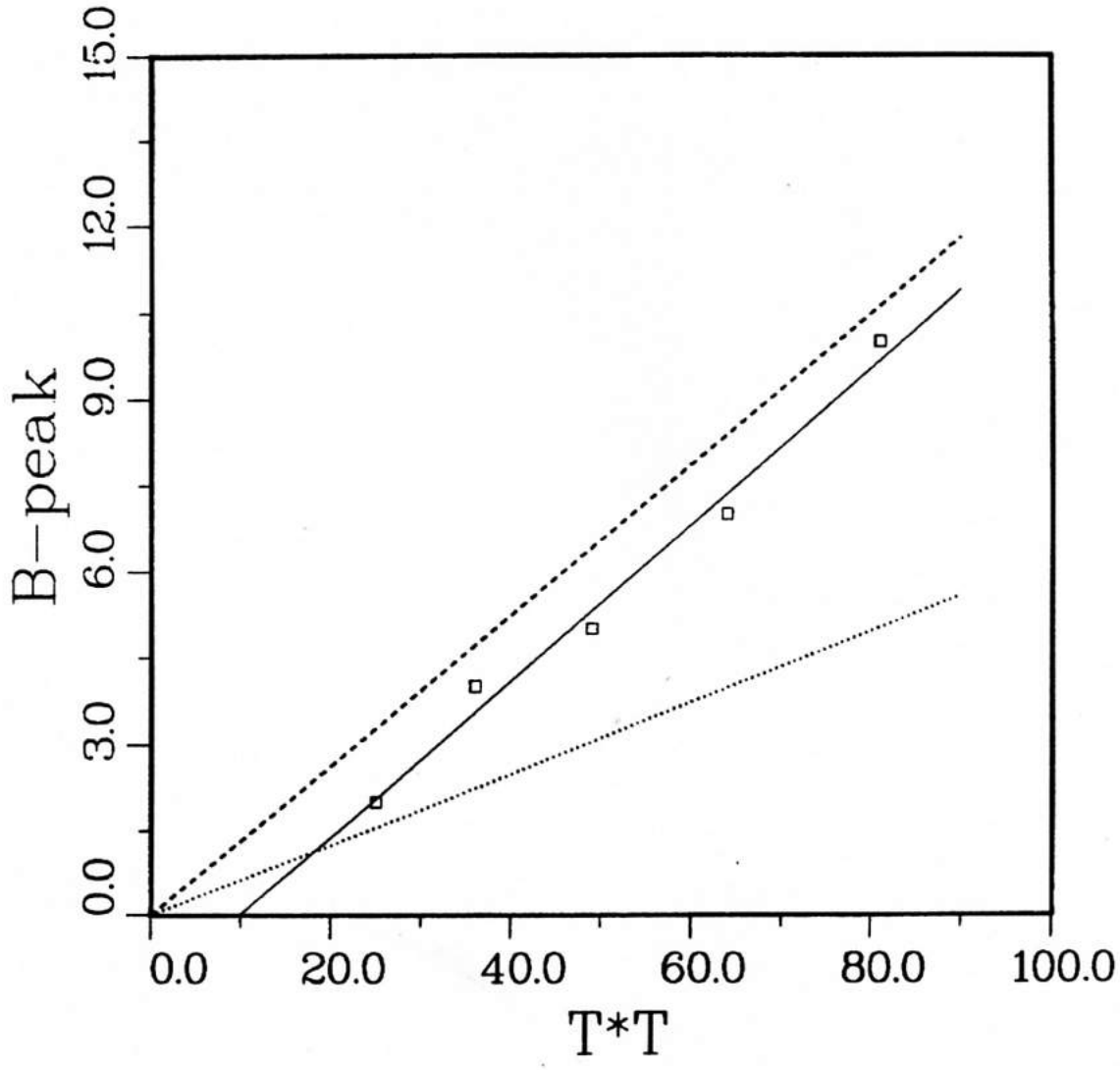

Figure 9.4 The field B_{peak} at which $\Delta C(B)$ is maximum for the $CsNiF_3$ parameters, vs. the square of the temperature (in kG and K^2 respectively). The data points are from the quantum M.C. calculation, and the solid line is a linear fit to that data. The dashed line is the linear fit to the Ramirez data, and the dotted line is the sG theory prediction.

where one cannot infer much from the M.C. data due to the scatter. This agreement could be coincidental, however, due to the following possible reasons: i) The M.C. simulation has been done for a system with only 16 spins, and certainly it would be useful to do a further set of computations at a series of lattice sizes in order to investigate the finite size effects. From the spin-$\frac{1}{2}$ data, however, changing N would probably have a larger effect on the peak heights than on the peak positions; ii) The large statistical error in the M.C. data makes any conclusions drawn rather weak, and implies some errors in the estimated peak positions. This is attributed to a freezing of the simulation, especially for low temperature; iii) All of the M.C. data has been produced in the finite mT Trotter approximation. Obviously, to get exact results one needs to let $m \to \infty$. Therefore the major sources of error are expected to be finite N, finite m, and the finite length of the M.C. set of states generated.

The major drawback of this algorithm is its inefficiency -- one needs to find a way to greatly improve the acceptance rates for the individual moves in order to reduce the statistical errors. Also, the freezing of the system at low temperature is a serious problem and might be corrected by an annealing procedure.

Because of these problems with the method we cannot make any strong conclusions, especially concerning the question of a "quantum soliton" interpretation to the experimental data. Also, we cannot verify the applicability of the assumed Hamiltonian and its parameters for a description of $CsNiF_3$. However, it is likely that quantum effects <u>are</u> important in this spin-1 material, and further careful study would be in order, possibly by evaluation of the thermodynamic properties via a transfer matrix approach on the 2-D effective lattice.